Light-Scattering Study of the Sol-Gel Transition in Silicon Tetraethoxide

M. Dubois and B. Cabane*

Departement de Physico-Chimie, Centre d'études nucléaires de Saclay, 91191 Gif sur Yvette, Cedex, France. *Received March 21, 1988; Revised Manuscript Received November 30, 1988*

ABSTRACT: Branched siloxane polymers are obtained through the hydrolysis and condensation of silicon tetraethoxide (TEOS) monomers in ethanolic solutions; they grow and end up forming a macroscopic network that entraps the solvent. At various times during the reaction, the sizes of individual polymers and their relative locations in the reaction bath are examined through light scattering. We find that the polymers grow with fractal structures and that smaller ones fill the voids of larger ones. This interpenetration is characterized by a screening length ξ, beyond which the internal correlations of one polymer are screened by the correlations between distinct polymers: ξ is the size of the largest lumps or voids in the reaction bath. These lumps and voids keep growing through the gel point and beyond, because the smaller polymers which fill voids in the larger polymer's structures diffuse away and bind to denser regions. This process is absent from percolation models, and it is controlled by the catalysis of the reaction. Hence large and small polymers have different roles in gel formation: large ones control the connectivity of the bath and smaller ones control the spatial variations of its density.

Introduction

Inorganic gels can be made by polymerization of organometallic precursors dissolved in an alcoholic solvent. They are used as intermediates in the sol-gel-glass processes for manufacturing oxide materials such as glasses, glass ceramics, and ceramics.[1-18] Using sol-gel routes rather than the traditional, high-temperature routes is an attractive idea, as it offers a better way to control the material's compositions and textures.[5-12,18-24] The first point depends on controlling the reactivities of the different monomers used in the reaction: this is chemistry. The latter one depends on controlling the spatial variations of the density of polymer segments, so as to suppress the formation of voids and lumps on some scales and enhance it on other scales: this is physics.

In the work reported here the chemistry is comparatively simple, since there is only one type of monomer, which is $Si(OC_2H_5)_4$, named silicon tetraethoxide (TEOS). Still, there are many ways in which TEOS monomers can be polymerized, mainly because the Si atoms, which have fourfold coordinance, are incompletely linked to each other in the polymerization reaction. For example, in TEOS/water/ethanol mixtures with molar ratio 1/10/5.8, the number of siloxane bridges rises to 70% of its value in dense silica, but the resulting gels have a volume 27 times that of dense silica.[13,14] As we use somewhat similar conditions, we expect that the polymers will grow largely branched but not dense.

Of course the structure of the gel depends not only on how many links are made but also on the relative locations of these links and on their topology (how are they connected).[25-31] Small-angle scattering methods can provide statistical information on these problems. Indeed, the small-angle scattering pattern measures pair correlations between all fluctuations in the density of polymer segments throughout the irradiated volume.[32,33] In the reaction bath, we obtain some parameters of the lumps and voids which form as the polymers move close to each other or away from each other. In diluted solutions, where the polymers have been separated from each other, we find out which groups of atoms are mechanically coherent and which ones can move (freely) past each other. We have already reported neutron-scattering experiments which analyze such correlations in the range 60-1000 Å for a concentrated TEOS reaction bath and for the diluted solutions extracted from it.[34] Here we present a similar study through light scattering, which allows the measurement of correlations at larger distances (1000-10 000 Å).

Polymerization of TEOS in Water/Ethanol Mixtures

The polymerization of TEOS can be obtained through hydrolysis of the ethoxy groups into silanols, followed by a condensation of the silanols to form the siloxane bridges.[1-3,13-17] We use conditions where the hydrolysis is fast and complete, whereas the condensation is slow and incomplete.

A cold solution of freshly distilled monomer (1 mol) in ethanol (7 mol) is added dropwise to a cold water (8 mol)/HCl mixture under slow agitation; the hydrolysis is catalyzed by the H^+ ions, and the amount of water is in excess of that needed for hydrolyzing all ester groups into silanols. The hydrolysis is exothermal and brings the temperature of the mixture back to room temperature; it is complete in less than 1 h. At this point, the reaction bath is placed in an oven at 50 °C; the silanols then condense to form siloxane bridges between the silicon atoms and release some of the water used for the hydrolysis.

We made one polymerization at a pH value much above the isoelectric point of SiOH (pH 4.64 after mixing, rising to 5.1 after hydrolysis); the condensation then proceeds through a nucleophilic attack of a silicon by the oxygen of a SiO^- group.[1-4] The gelation is fast (13 h at 50 °C); it gives a gel which is slightly turbid and does not tend to shrink as it ages beyond the gel point. The weight concentration of silica in the swollen gel is 0.08 g/cm^3, and its volume fraction (assuming a density of 2 g/cm^3) is 0.04.

The other polymerization reactions were made at a pH value somewhat below the isoelectric point of SiOH (pH 1); then the silanols are protonated into $SiOH_2^+$, which tends to decrease the nucleophilic character of the oxygen and prevent it from attacking another silicon. Nevertheless the condensation was still weakly catalyzed, because the H^+ ions help the release of a water molecule from the newly formed dimers. The gelation times were 180-220 h at 50 °C; the resulting gels were completely transparent and did tend to shrink through syneresis.

The gelation times are notoriously difficult to reproduce. The main problem is in controlling the pH of the reaction bath, especially when the concentration of H^+ ions is low

0024-9297/89/2222-2526$01.50/0

(pH 5). Another problem may result from heterogeneous polymerization conditions, where the concentration of catalyst or that of reacting species may not be the same throughout the reaction bath. This last point deserves special mention, because it is not always appreciated. Indeed, the rate of the condensation depends very strongly on the separation of reacting species.[35-37] Because of this concentration dependence, the polymerization will be extremely fast near surfaces where solvent evaporation raises the monomer concentration near unity. These highly polymerized species can be produced in films that wet the walls of the container or in free surfaces; if they are washed into the reaction bath, they will dominate the scattered intensities. It is therefore necessary to eliminate all free surfaces if the experiments are to describe the gelation of a bulk phase.

Light-Scattering Measurements

At various times during the polymerization reaction, a small fraction of the reaction bath is extracted and examined through light scattering. Then it is diluted with ethanol, and the light-scattering spectrum is taken again. Successive dilutions bring the polymer concentration down to 6/10, 3/10, 1/10, ..., 3/1000 of the original concentration in the reaction bath. None of these solutions is filtered, for fear of eliminating some large polymers which would be intrinsic to the gelation process; on the other hand, all reagents have been filtered before the reaction, and all manipulations are performed in a dust-free hood.

For light-scattering measurements, the solutions are placed in a 2.5-cm cylindrical test tube at the center of a 9-cm cylindrical cell filled with toluene. The light source is an argon ion laser, operated at a wavelength $\lambda = 5145$ Å with a power of 0.1–1 W. The incident light is vertically polarized and focused on the sample through a 100-mm lens; neutral density filters are used to reduce the incident intensity for solutions or gels which are strong scatterers. The scattered light is collected through a system of slits, which defines the scattering volume; it is focused on a Thorn EMI photomultiplier whose position with respect to the beam is controlled by an Amtec MM1 goniometer. The output of the PM is sent to a Malvern multibit correlator; for measurements of the static intensity this instrument just integrates the number of pulses per unit time.

The measured intensities are corrected for the variation of the scattering volume with scattering angle θ and divided by the incident intensity; then they are compared with the intensity scattered by the pure solvent and normalized by the intensity scattered from liquid benzene in the same conditions:

$$I_{abs}(\theta) = [I_{solution}(\theta) - I_{ethanol}(\theta)]/I_{benzene}(\theta)$$

Finally, the data are sorted according to the magnitude of the scattering vector $\mathbf{Q}$, which is

$$Q = (4\pi(n/\lambda)) \sin(\theta/2)$$

where n is the index of refraction of the scattering medium (1.36 for ethanol) and λ the wavelength of the incident radiation. The range of accessible angles is 10–160°, giving Q values between 0.3×10^{-3} and 3.3×10^{-3} Å^{-1}.

For diluted solutions, these absolute intensities yield the average mass M_w and radius R_z of the polymers through an expansion at low Q and low c according to the Zimm formula:[33,38]

$$\frac{K'c}{I(Q)} = \frac{1}{M_w}\left(1 + \frac{Q^2R_z^2}{3}\right) + 2A_2c$$

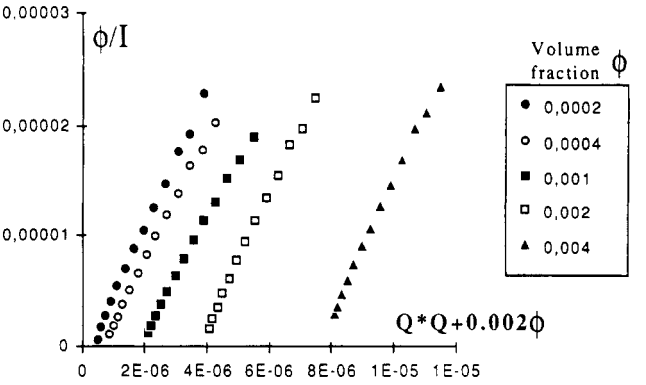

Figure 1. Zimm plot for the dilute solutions extracted at t = 213 h from a reaction bath at pH 1. Vertical scale: ϕ/I, where ϕ is the volume fraction of polymer in each dilution, and the intensity I is divided by that of benzene. Horizontal scale: $Q^2 + 0.002\phi$, with the magnitude of the scattering vector, Q, in Å^{-1}.

The constant K' is determined by the increment of index of refraction (dn/dc) for the TEOS polymers in ethanol:[38]

$$K = 2\pi^2\lambda^{-4}n_B^2(dn/dc)^2R_BN_A^{-1}$$

where R_B is the Rayleigh ratio of benzene, equal to 32.05×10^{-6} cm^{-1} at $\lambda = 5145$ Å and 25 °C, and N_A is Avogadro's number. We have measured dn/dc for the solutions extracted from the reaction bath at pH 1; the measured value is 0.126 cm^3/g. With these values the constant K is equal to

$$K' = 5 \times 10^{-3} \text{ cm}^3 \text{ mol g}^{-2}$$

The formula which gives the scattered intensity as a function of average parameters for all the polymers in the solution is valid only if Brownian motions of the macromolecules produce a proper thermal average in the irradiated volume over the integration time. This thermal averaging fails in concentrated solutions of very large polymers and in gels; the measured intensities then take a chaotic behavior, which is controlled by the internal structure and motions of macroscopic objects. A fair amount of averaging can be restored by integrating over a larger volume, for example by rotating the sample. Then, close to the gel point, the main limitation is that dilutions cannot be performed or that they do not give a representative sample of the reaction bath.

Scattering from Dilute Solutions

When the reaction bath is diluted to volumes much beyond its original volume, the polymers are separated from each other. This has two important consequences. Firstly, the encounters between polymers become rare, and the reaction is effectively quenched.[39] Secondly, the positions of individual polymers are no longer correlated, and therefore all interferences between them average out in the scattering pattern. Consequently the intensity scattered by a dilute solution is just the average of the intensities scattered by individual polymers. Specifically, the $Q \to 0$ limit of the intensity yields the weight-averaged mass M_w of the polymers, and its curvature at low Q yields their z-averaged radius R_z.[33,38]

Figure 1 shows our results for solutions extracted from a reaction bath at pH 1 after 173 h at 50 °C (gelation occurred at 180 h); Figure 2 shows the data for a reaction at pH 5 during 12 h at 50 °C (gelation at 13 h). Here the data are plotted in the Zimm representation ϕ/I vs Q^2, where ϕ is the volume fraction of polymer in the reaction bath; the curves corresponding to different concentrations are shifted along the horizontal axis to allow an extrapolation to infinite dilution. Each scattering curve yields an

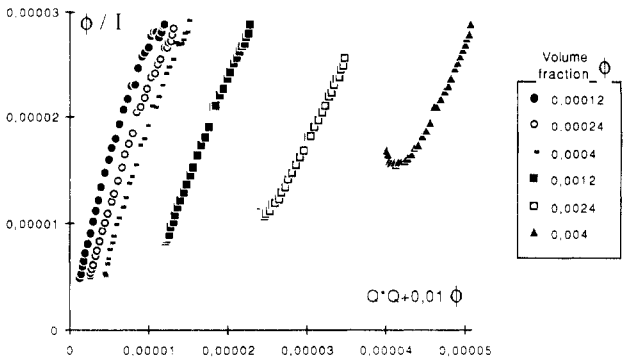

Figure 2. Zimm plot for the dilute solutions extracted at t = 12 h from a reaction bath at pH 5. The curvature observed at high volume fraction and low Q is caused by repulsions between the individual polymers.

Table I
Parameters of the TEOS Polymers in Dilute Ethanolic Solutions[a]

sol	pH	time, h	M_w	A_2	R_z	Ψ
Q	1	93	8.5 E4	3.6 E-4	144	0.06
P	1	168	5.9 E5	1.4 E-4	345	0.09
Q	1	164	1.3 E6	6.25 E-5	471	0.08
P	1	190	1.9 E6	3.5 E-5	565	0.05
O	5	12	1.14 E7	1.55 E-5	1400	0.05
P	1	213	8.2 E7	2.25 E-6	3043	0.04
b			5.63 E7	1.09 E-4	5060	0.23
b			1.23 E6	2.86 E-4	509	0.25

[a] M_w is the weight-average molar mass, R_z the z-averaged radius in Å, A_2 the second virial coefficient in cm^3 mol g^{-2}, and Ψ the interpenetration coefficient, which normalizes A_2 to the volume of each macromolecule.[42] [b] Polystyrene/C_6H_6 (values taken from ref 42).

apparent mass and an apparent radius for the polymers; these values are affected by correlations between different polymers and therefore depend on concentration. The values extrapolated to infinite dilution are the proper averages over individual polymers, and the slope of the extrapolation yields the second virial coefficient A_2, which measures the two-body interactions between distinct polymers.

All these values are listed in Table I and are compared with those for solutions of monodisperse, linear polymers in a good solvent (polystyrene in benzene). Here the main differences are in the values of the second virial coefficient A_2, which indicate strong correlations for monodisperse, linear macromolecules and weaker correlations between polydisperse, randomly branched TEOS polymers.

Figure 3 shows the variation of the second virial coefficient A_2 with M_w: the slope (0.73) is close to that predicted for polydisperse, randomly branched polymers,[30] much stronger than that for monodisperse, linear polymers. Figure 4 shows the variation of the z-average radius R_z with the weight-average mass M_w; the slope of this plot gives an apparent fractal dimensions D while the intercept depends on the mass and size of the statistical unit of a polymer chain:

$$M/m = (R/a)^D$$

From the values of M_w and R_z measured at different times in the reaction bath at pH 1, we find that the statistical unit is comparable to the monomer (m = 61 for a = 4 Å); hence the polymer strands do not coalesce into fibers, films, or globular subunits. The fractal dimension D is close to 2; this value is not particularly meaningful, since it reflects not only the internal structure of the polymers but also their size distribution. Similar values

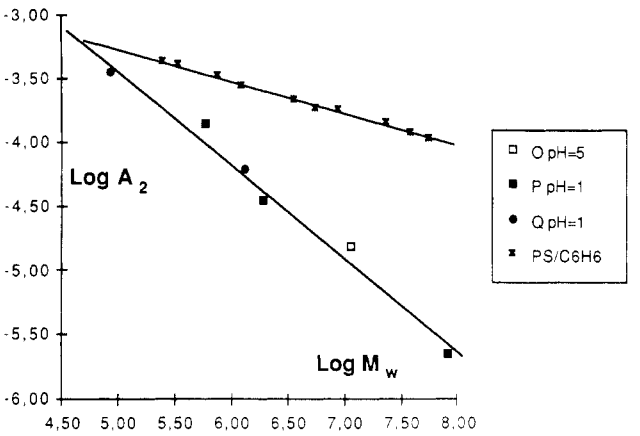

Figure 3. Second virial coefficient for the interactions between distinct macromolecules in dilute solutions. This coefficient measures the correlations in position which are caused by repulsions between neighboring macromolecules. For a given concentration, macromolecules of higher molecular weight do not get as much in each other's way, hence the downward slope of the plots. This effect is stronger for branched (TEOS) polymers than for linear ones (polystyrene in benzene) because they grow with a higher fractal dimension. Data for polystyrene from ref 42.

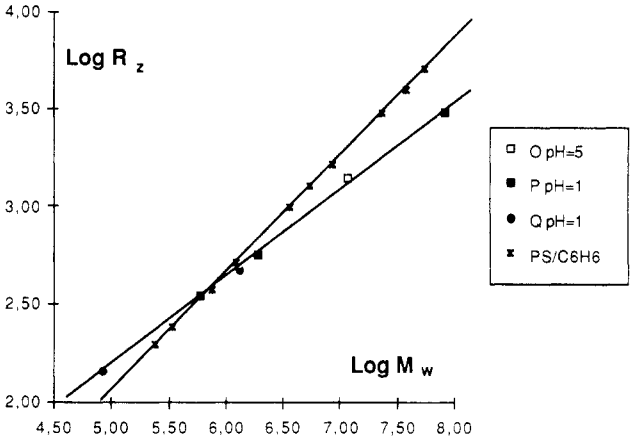

Figure 4. Radius of gyration vs molecular weight for polymers extracted at different times from TEOS reaction baths. The molecular weights are calculated from the intensities extrapolated to $Q \to 0$ and $\phi \to 0$ in the Zimm plots and the radii from the slopes of the Zimm plots, also extrapolated to infinite dilution. Both are averages heavily biased toward the largest polymers of the size distribution, especially so for the radii. The data show that TEOS polymers grow with a higher fractal dimension (D = 1.95) than linear macromolecules in a good solvent (polystyrene).

are obtained from the exponent of $I(Q)$ vs Q at higher Q values.[34]

Here the central result is that the average sizes and masses become quite large in the vicinity of the gel point. This phenomenon is not unexpected, since some polymers must become macroscopic for the sample to become a gel.[7,25-31] However, it had not been widely appreciated so far in aggregating systems, because most authors were concerned with the sizes measured in the reaction bath, which do remain microscopic right up to the gel point,[4,11,23,40,41] more on this later. Besides, it is interesting to note that for comparable degrees of polymerization the dilute solutions extracted from either reaction bath (pH 1 or pH 5) are quite similar: same statistical unit, same apparent fractal dimension D, and same virial coefficient. Hence the differences between these reaction baths (one is clear, the other turbid) do not show up in the very large polymers, which can be extracted from them by a dilution experiment.

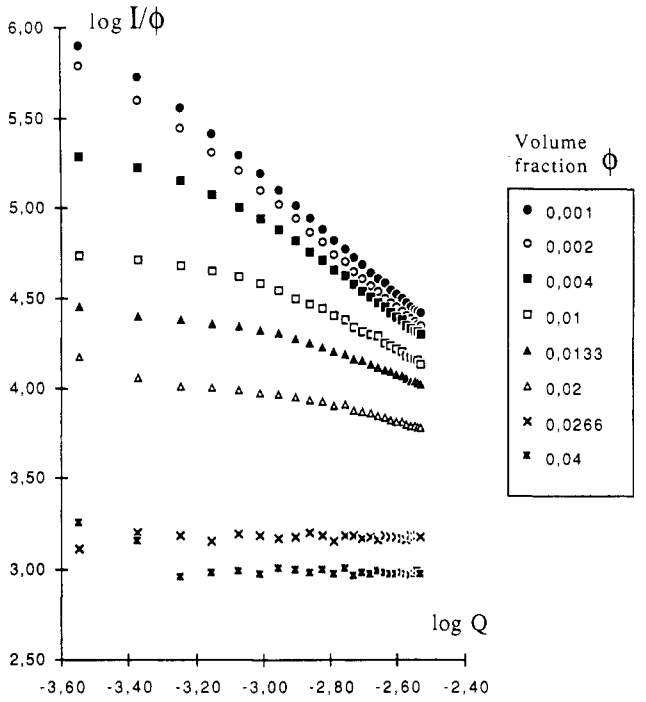

Figure 5. Angular dependence of the intensities for the solutions extracted at 173 h from the reaction bath at pH 1. Vertical scale: $\log_{10}$ (intensity/volume fraction). Horizontal scale: $\log_{10}$ (scattering vector Q). The top curve is from a very dilute solution, where the polymers are essentially noninteracting; the next curves are from the solutions where correlations between repelling macromolecules depress the scattered intensities. The last curve is from the reaction bath, where the macromolecules are extensively interpenetrated.

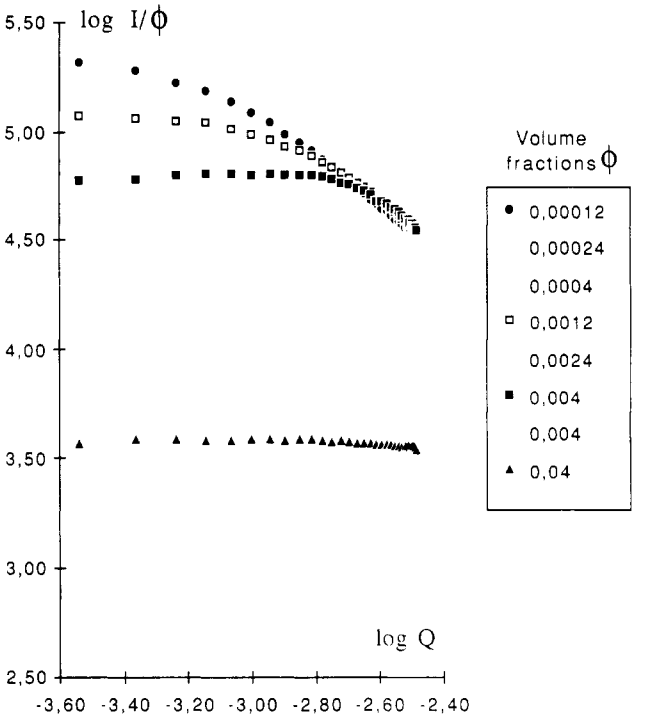

Figure 6. Angular dependence of the intensities for solutions extracted at 12 h from the reaction bath at pH 5. The top curve is from a very dilute solution, where the polymers are essentially noninteracting; the bottom curve is from the reaction bath. The depression of intensities at high volume fractions is much weaker than in the reaction baths at pH 1.

Scattering from Semidilute Solutions

At higher concentrations the scattering patterns are dominated by the effects of correlations between neighboring polymers. Because of such correlations, the interferences between rays scattered by distinct polymers do not average out, and the values of I/ϕ are truly depressed with respect to the dilute solution values (Figures 5 and 6). This effect is strongest in the $Q \rightarrow 0$ limit; for relatively dilute solutions it is measured by the second virial coefficient, which is mentioned above. Now for much higher concentrations, the interferences between distinct polymers become so strong that the values of I/ϕ decrease even faster, and the values of I also decrease with increasing ϕ. This effect is apparent in both reaction baths, but it is much stronger in the reaction bath at pH 1, indicating that the repulsions are much more effective in the latter. The volume fraction ϕ^*, where the intensity reaches its maximum value, marks the crossover between the dilute regime, where the polymers are only weakly correlated, and the semidilute one, where they are strongly correlated.

The Q dependence of the intensity in the semidilute range is also interesting. In all cases, the depression is strongest in the $Q \rightarrow 0$ limit, because at sufficiently high Q values the correlations within one macromolecule will dominate. In some cases, the low Q depression may be so sharp that there is a peak in $I(Q)$. Such peaks are commonly observed in concentrated dispersions of objects which resist interpenetration, thereby producing a hole in the pair correlation function for their center to center distances.[43] Here the peak position yields an estimate of the range ξ of the correlations; at distances larger than ξ the repulsions suppress the fluctuations in the density of polymer segments, and the solutions appear uniform. In other cases there is no peak, and the range of correlations is obtained from the curvature of the intensity at low Q (i.e., from a plot in the Zimm representation, as in the dilute range). The correlation lengths measured near the gel point are all much shorter than R_z: for the reaction baths at pH 1, ξ = 177 Å (Q), 150–200 Å (P), and 116 Å (K); for the bath at pH 5, ξ = 165 Å (O). Figure 7 shows the full variations of I and ξ with concentration (bath P, pH 1).

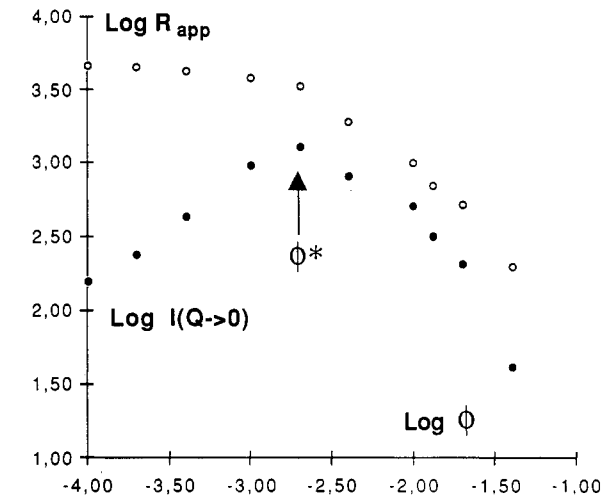

Figure 7. Effect of concentration on the intensities scattered at $Q \rightarrow 0$. For solutions of noninteracting polymers, the intensities would remain proportional to volume fraction (slope = +1), and the apparent radii would remain identical with the average radius R_z of individual polymers. Before ϕ^*, this is almost the case, with a slight deviation caused by repulsions between neighboring polymers. Beyond ϕ^*, the polymers overlap despite their repulsions; the combination of interpenetration and repulsions reduces the extent of refractive index fluctuations.

Evolution of the Reaction Bath

As the reaction progresses and the individual polymers become quite large (Table I), the sizes ξ which are mea-

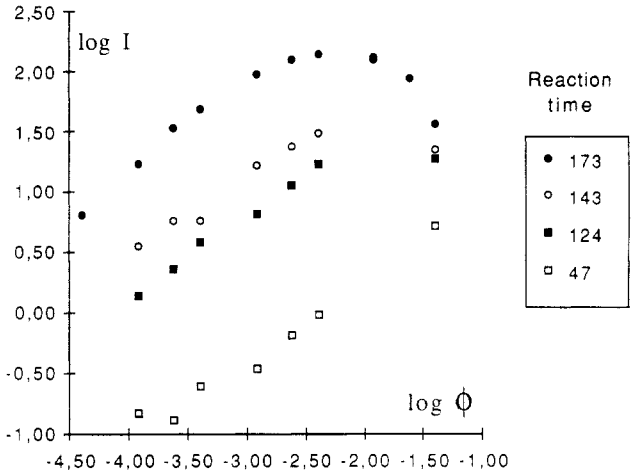

Figure 8. Concentration dependence of intensities for the solutions extracted at different times from the reaction bath at pH 1. Scattering angle 30°, $Q = 0.866 \times 10^{-3}$ Å^{-1}. Lower curve: t = 47, 124, 143, 173 h. As the polymers grow, the dilute regime where I rises with ϕ is pushed down to lower volume fractions.

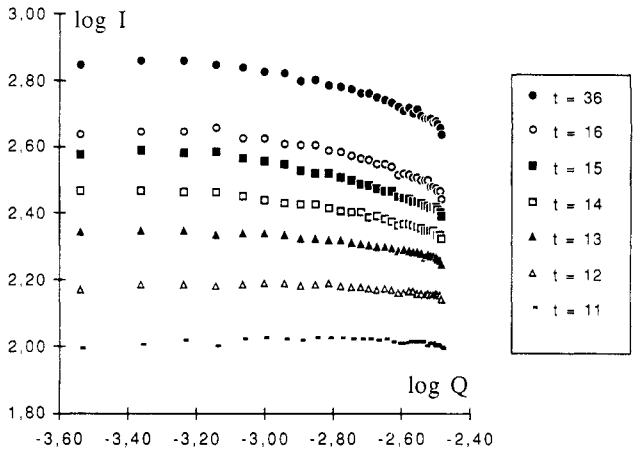

Figure 9. Evolution with time of the reaction bath at pH 5; this sample gelled at t = 13 h. The angular dependence of the scattered intensity becomes more pronounced at later times, indicating that the scattering is caused by larger objects.

sured in the bath remain microscopic, and the corresponding intensities are much below the sum of the individual intensities. In this way the reaction bath remains relatively transparent even though it contains some very large objects. This effect is demonstrated in Figure 8, where the I vs ϕ curves are compared at different times before t_g. On the dilute solution side, as the polymers become larger, they also get in each other's way sooner, and consequently the range of dilute solutions is pushed down to lower volume fractions. On the concentrated side, these correlations between neighboring polymers depress the intensities down to a value characteristic of microscopic domains. This is another indication of repulsions which force the density of polymer segments to remain uniform at sizes beyond ξ.

The intensities scattered by the reaction bath still do rise, indicating that the bath grows larger lumps and voids. This is shown in Figure 9, where the apparent size ξ of the scattering units rises from 165 Å at t = 11 h, before t_g, to 400 Å at t = 36 h $\approx 3t_g$. Hence the growth of heterogeneities in the bath is not associated with its sol–gel transition.[34] Rather it implies that polymer segments are removed from low-density regions and bound to high-density regions. This involves a depletion of smaller polymers through binding to larger polymers and a densification of the larger ones.

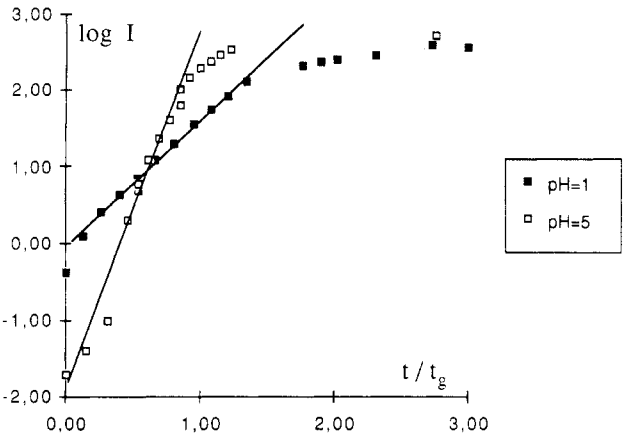

Figure 10. Intensities vs time for both reaction baths on semilog scales. Scattering angle 90°, $Q = 2.37 \times 10^{-3}$ Å^{-1}. At the gel point the intensities scattered by the reaction bath do not show any singularity.

The time dependence of this growth is displayed in Figure 10. Here the time scales are expressed in reduced units t/t_g; the growth of heterogeneities is then much faster in the bath at pH 5. The law appears to be exponential in time, with a saturation at long times.

Discussion

Our results follow the empirical finding that gelation can follow many different courses. In sol–gel processes, this variability occurs because gelation is a consequence of segregation: monomers or polymers segregate from the solvent as they bind to form larger units, and the rules of this aggregation are set by the relative rates of all possible condensation reactions.

Two types of information are needed: where the polymers are with respect to each other when they bind or when they fail to do so; which types of polymer are formed through these recombination reactions. Scattering provides statistical information on both problems: experiments on very dilute solutions give the average mass and size of individual macromolecules. Experiments on more concentrated solutions yield interference patterns from relative configurations of neighboring macromolecules.

Concerning *individual macromolecules*, we find that the polymers grow as fractal objects (Figure 3), whose masses and sizes diverge at the gel point (Table I). The laws for this divergence have been determined by other workers;[7] it has been found that this information is not enough to determine the nature of the gelation process (e.g., kinetic aggregation or percolation). Presumably more detailed information is needed to solve the problem from this end; for instance, measuring the full distribution of masses and sizes would allow one to proceed back to the kernel of the Smoluchovski equation.

Concerning the relative configurations of *neighboring macromolecules*, we also expect that they will be determined by their size distribution and by their fractal dimension (distribution of voids in the structure of each macromolecule). In our experiments we find two behaviors according to the polymer concentration: a dilute range ($\phi < \phi^*$), where adding more polymer still raises the intensities, and a semidilute range ($\phi > \phi^*$), where the intensities decrease with increasing concentration. The classic interpretation of these two ranges is found in the paper by Daoud and Leibler.[30] In dilute solutions, neighboring macromolecules repel and do not overlap; in semidilute solutions, osmotic pressure drives the smaller ones into the voids of larger ones, so that the fluctuations of refractive index decrease when more polymer is added to the solu-

tion. We now discuss these two ranges in turn.

Dilute Solutions. In this range the osmotic pressure of polymer segments is low, and the polymers need not interpenetrate; their correlations are determined by the loss of accessible configurations caused by these repulsions.[43] The resulting correlations must be quite strong, for instance, when the segment concentration is 2×10^{-3} and the intensities are 10 times lower than the sum of intensities scattered by individual macromolecules (Figure 4). This loss of configurations appears as a forbidden region in the pair correlation function $g(r)$, which in turn produces the depression of $I(Q)$ at low Q.[44] For instance, if the polymers are all of the same size, the forbidden region will be comparable to the polymer size, and the intensities will be strongly depressed at low Q. More generally, the existence of a forbidden region in $g(r)$ is associated with a lower cutoff in the distribution of polymer sizes.[45] Accordingly, the differences observed at moderate concentrations (0.004) between both reaction baths must reflect the lower cutoffs in their respective size distributions.

Semidilute Solutions. At higher concentrations, the osmotic pressure of polymer segments forces the smallest polymers into the voids of the largest ones. This combination of repulsions and interpenetration leads to a screening effect in the sense of Edwards[46] and Jannink and de Gennes,[47] because remote sections of one macromolecule are screened from each other by strands of another macromolecule. The spatial range of correlations (lumps and voids) produced by one macromolecule is now shorter then R_z: it is limited to a screening length ξ, which is the average distance between strands of distinct macromolecules. The main difference with the Edwards–de Gennes picture is that interpenetration is controlled by the size distribution, since branched polymers of the same size cannot overlap.[48]

A formal way of describing such solutions is to separate the polymers into discrete classes of increasing sizes. We start near the overlap concentration ϕ^*, where the sum of volumes which are spanned by individual polymers equals the total volume of the solution:

$$\sum_{n_{min}}^{n_{max}} v_i = V_0$$

Above ϕ^*, the polymers must overlap; as mentioned above, the largest ones will be penetrated by the smallest ones. We keep in one class all the smallest polymers, including enough of them to reach ϕ^* condition (Figure 11). Then the larger ones are fully penetrated, and we can assume that they do not contribute to the scattering. In this approximation, the largest lumps or voids which can be observed correspond to the largest polymers that are not penetrated by others, at the limit between the two classes. This size is the spatial correlation length or screening length ξ.[28,30] At still higher concentrations we can separate more than one class of polymers which meet the ϕ^* condition, because each class contains a narrower range of polymer sizes:

$$\sum_{n_{min}}^{n_1} v_i = \sum_{n_1}^{n_2} v_i = \ldots = V_0$$

In each of these classes the polymers are penetrated by smaller ones from the previous class, and they penetrate the larger ones from the next class. Still, the spatial correlation length ξ remains defined as the size of the largest polymers which are not penetrated by others (n_1), at the limit between the first class and the next one. It will of course become shorter at higher concentrations, as

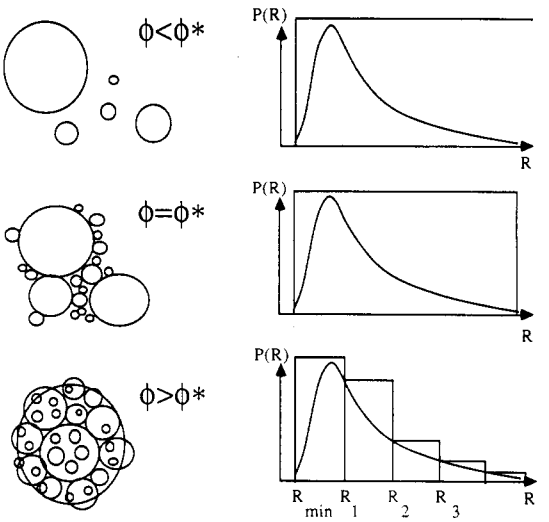

Figure 11. Interpenetration of fractal polymers with a broad size distribution. Polymers of the same size repel each other, but at high concentrations the osmotic pressure drives smaller ones into the voids of larger ones (left-hand side, where the polymers are represented by their outer boundaries). Polymers which do not overlap are regrouped in discrete classes (right-hand side and text); in each class the polymers are penetrated by polymers of the previous class, and they penetrate polymers of the next one.

n_1 moves closer to n_{min}, because all classes become narrower; this is the observed behavior (Figure 6).

The main virtue of this decomposition is that it shows which aspects of gelation can be universal and which ones will not. The right-hand side of the size distribution (Figure 11) can show universal features, because of the self-similar nature of the growth process; hence we expect universal exponents for the connectivity of the reaction bath. Also, the existence of screening effects is related to the self-similar succession of interpenetrated classes, and as such it is now part of the standard lore of gelation.[27–31,49–51] On the other hand, the actual values of the screening length and of the intensities scattered by the bath are determined by the left-hand side of the size distribution. This a low molecular weight cutoff controlled by the depletion of the smallest polymers as they recombine or are captured by larger ones; such processes have no reason to be universal. Hence *the spatial correlations in the reaction bath are not universal, because they are controlled by the smaller polymers of the size distribution.*

Now we are in a position to discuss the main issues of sol–gel processes: (i) the growth of lumps and voids in the reaction bath as the reaction progresses through the gel point and beyond and (ii) the effect of catalysis on this growth.

The *growth of lumps and voids* is obvious from the beginning of the reaction, and it continues in conditions where the polymers are largely overlapped. For instance, Figure 8 shows that beyond $t = 0.8t_g$ the reaction bath is in the overlapped regime ($\phi > \phi^*$), yet Figures 9 and 10 show that the growth continues much beyond t_g. This is in conflict with most current models of the sol–gel transition, basically because they do not describe the appropriate size distribution for the polymers. In monodisperse models, the apparent size grows, but it stops at the gel point when all polymers come into contact. In site or bond percolation, the dilutions made at a fixed concentration will give a constant spatial correlation length because there are so many small polymers and so few large ones that gelation can occur without depleting substantially the bath of smaller polymers. Finally in correlated correlation, the spatial correlation length does grow, but this is a conse-

quence of a phase separation where the gel would separate from its solvent; in the present case the polymers are always in a good solvent (see the positive values of the second virial coefficient, Table I). There is no sign of the divergence of ξ which is predicted by this model: the correlation length just saturates at long times when all polymers are bound or trapped.

To understand this problem, it is useful to refer again to the picture where the polymers are sorted out in discrete classes according to their sizes (Figure 11). The lumps and voids observed correspond to the correlations of polymers in the first class; by definition these polymers are not interpenetrated, and they are densely packed in the bath. Now consider a later stage of the reaction, where the size, ξ, of lumps and voids has grown to a larger value: this is a consequence of recombination processes, by which all polymers in the first class become larger. However, in the same process they also must acquire a higher fractal dimension, D. This is clear from the behavior of the pair correlation function $g(r)$, which decays with an exponent $3D$ from a fixed value $g(a)$ at the origin to a fixed value at $r = \xi$ because $g(\xi)$ is set by the average density of the bath. We have observed this crossover in small-angle neutron scattering experiments,[34] where the apparent fractal dimension is 1.7 near the gel point and rises to 2.3 at long times. In this respect, it is important to note that a slight change in D can result in a large increase in ξ; for instance, at $\phi = 0.04$, ξ will double if D goes from 2.25 to 2.35. From this we conclude that the growth of lumps and voids in the reaction bath goes together with a densification of the polymers in the later stages of the reaction, both effects being direct consequences of recombination processes in a solution of overlapped polymers. This is consistent with the results of numerical simulations in systems of finite density.[52]

Finally, we still need to understand how this growth of lumps and voids depends on the catalysis of the reaction. This is essential if we are to control the structure of gels by manipulating the conditions of the reaction. The effect is clearly seen by comparing the intensities scattered from both reaction baths (Figures 4 and 5); even though the intensities scattered by dilute solutions are comparable, the reaction bath at pH 5 scatters 5 times more, and it is much more turbid. This is certainly related to the detailed shape of the size distribution and therefore to the kernel of the Smoluchovski equation for each type of catalysis, where the rate coefficients describe whether large polymers grow through capture of smaller ones or whether polymers of the same size tend to recombine together. The key to the problem presumably lies with the old Brinker argument,[3,4] according to which the former processes are favored at high pH and the latter ones at low pH. However, it may be better to first measure accurately the size distribution and then draw conclusions accordingly; such measurements are in progress.

Conclusion

The spontaneous recombination of polymers which are dissolved in a solvent is a hazardous route to gelation because it allows the possibility of some regions getting densified and others depleted. In general, all such gels will be nonuniform (and therefore turbid) unless interpenetration and repulsions of neighboring polymers limit the fluctuations in the density of polymer segments. This screening effect is controlled by the smaller polymers in the size distribution; as they are depleted through recombination reactions, the apparent size of lumps and voids in the reaction bath becomes larger.

As a result, sol–gel processes show an unusual mixture of universal and nonuniversal features. The connectivity of the reaction bath, which is controlled by the largest polymers in the size distribution, follows universal laws; the spatial distribution of polymer segments in the bath, which is controlled by the smallest polymers, behaves in ways that are not universal and depends on the catalysis of the reaction.

Acknowledgment. This work benefited from essential ideas and critical comments by M. Adam, M. Daoud, M. Delsanti, J. F. Joanny, and L. Leibler. It is a pleasure for us to acknowledge their share in this field.

References and Notes

(1) Aelion, R.; Loebel, A.; Eirich, F. *J. Am. Chem. Soc.* **1950**, *72*, 5705.
(2) Engelhardt, G.; Atlenburg, W.; Hocbbel, D.; Wicker, W. *Z. Anorg. Allg. Chem.* **1977**, *428*, 43.
(3) Brinker, C. J.; Keefer, K. D.; Schaefer, D. W.; Ashley, C. S. *J. Non-Cryst. Solids* **1982**, *48*, 47.
(4) Brinker, C. J.; Keefer, K. D.; Schaefer, D. W.; Assink, R. A.; Kay, B. D.; Ashley, C. S. *J. Non-Cryst. Solids* **1984**, *63*, 45.
(5) Brinker, C. J.; Scherer, G. W. *J. Non-Cryst. Solids* **1985**, *70*, 301.
(6) Brinker, C. J.; Scherer, G. W.; Roth, E. P. *J. Non-Cryst. Solids* **1985**, *72*, 345.
(7) Martin, J. E.; Wilcoxon, J.; Adolf, D. *Phys. Rev. A* **1987**, *36*, 1803.
(8) Klein, L. C.; Garvey, G. J. *J. Phys. (Les Ulis, Fr.)* **1982**, *43*, C9-271.
(9) Klein, L. C. *Annu. Rev. Mater. Sci.* **1985**, *15*, 227.
(10) Dauger, A.; Chaput, F.; Pouxviel, J. C.; Boilot, J. P. *J. Phys. (Les Ulis, Fr.)* **1985**, *46*, C8-455.
(11) Pouxviel, J. C.; Boilot, J. P.; Lecomte, A.; Dauger, A. *J. Phys. (Les Ulis, Fr.)* **1987**, *48*, 921.
(12) Pouxviel, J. C.; Boilot, J. P.; Dauger, A.; Huber, L. Better Ceramics Through Chemistry 2. *Mater. Res. Soc. Symp. Proc.* **1986**, *73*, 269.
(13) Pouxviel, J. C.; Boilot, J. P.; Beloeil, J. C.; Lallemand, J. Y. *J. Non-Cryst. Solids* **1987**, *89*, 345.
(14) Pouxviel, J. C.; Boilot, J. P. *J. Non-Cryst. Solids* **1987**, *94*, 374.
(15) Artaki, I.; Bradley, M.; Zerda, T. W.; Jonas, J. *J. Phys. Chem.* **1985**, *89*, 4399.
(16) Orcel, G.; Hench, L. *J. Non-Cryst. Solids* **1986**, *79*, 177.
(17) Kelts, L. W.; Effinger, N. J.; Melpolder, S. M. *J. Non-Cryst. Solids* **1986**, *83*, 353.
(18) Dislich, H. *J. Non-Cryst. Solids* **1983**, *57*, 371.
(19) Dislich, H. *J. Non-Cryst. Solids* **1985**, *73*, 599.
(20) Zarzycki, J.; Prassas, M.; Phalippou, J. *J. Mater. Sci.* **1982**, *17*, 3371.
(21) Quinson, J. F.; Dumas, J.; Serughetti, J. *J. Non-Cryst. Solids* **1986**, *79*, 397.
(22) Dumas, J.; Quinson, J. F.; Bovier, C.; Serughetti, J. *J. Non-Cryst. Solids* **1986**, *82*, 220.
(23) Himmel, B.; Gerber, Th.; Bürger, H. *J. Non-Cryst. Solids* **1987**, *91*, 122.
(24) Doeuff, S.; Henry, M.; Sanchez, C.; Livage, J. *J. Non-Cryst. Solids* **1987**, *89*, 206.
(25) Flory, P. J. *Principles of Polymer Chemistry*; Cornell University Press: Ithaca, NY, 1953.
(26) Stockmayer, W. H. *J. Chem. Phys.* **1943**, *11*, 45; **1944**, *12*, 125.
(27) Stauffer, D. *J. Chem. Soc., Faraday Trans. 2* **1976**, *72*, 1354.
(28) de Gennes, P. G. *Scaling Concepts in Polymer Physics*; Cornell University Press: Ithaca, NY, 1979.
(29) Stauffer, D.; Coniglio, A.; Adam, M. *Adv. Polym. Sci.* **1982**, *44*, 103.
(30) Daoud, M.; Leibler, L. *Macromolecules* **1988**, *21*, 1497.
(31) Adam, M.; Delsanti, M.; Munch, J. P.; Durand, D. *J. Phys. (Les Ulis, Fr.)* **1987**, *48*, 1809.
(32) Debye, P.; Bueche, A. M. *J. Appl. Phys.* **1949**, *20*, 518.
(33) Zimm, B. *J. Chem. Phys.* **1948**, *16*, 1093.
(34) Cabane, B.; Dubois, M.; Duplessix, R. *J. Phys. (Les Ulis, Fr.)* **1987**, *48*, 2131.
(35) Yoldas, B. E. *J. Non-Cryst. Solids* **1986**, *82*, 11.
(36) Yoldas, B. E. *J. Non-Cryst. Solids* **1986**, *83*, 375.
(37) Pouxviel, J. C. Thesis, University Pierre et Marie Curie, Paris, 1987.
(38) Huglin, M. *Light Scattering from Polymer Solutions*; Academic Press: London, 1972.
(39) When the reaction bath is diluted in ethanol, its scattering pattern changes immediately and then remains stable more than 3 weeks.

(40) Schaefer, D. W.; Keefer, K. D. Better Ceramics Through Chemistry 1. *Mater. Res. Soc. Symp. Proc.* **1984**, *32*, 1.
(41) Orcel, G.; Gould, R. W.; Hench, L. L. Better Ceramics Through Chemistry 2. *Mater. Res. Soc. Symp. Proc.* **1986**, *73*, 289.
(42) Cotton, J. P. *J. Phys. (Les. Ulis, Fr.)* **1980**, *41*, L231.
(43) Branched polymers of similar sizes will repel each other. See: Daoud, M.; Joanny, J. F. *J. Phys. (Les Ulis, Fr.)* **1981**, *42*, 1359.
(44) Hansen, J. P.; Mc Donald, I. R. *Theory of Simple Liquids*; Academic Press: London, 1976.
(45) It is well-known that broader size distributions will reduce the depression in $I(Q)$. See for instance: van Beurten, P.; Vrij, A. *J. Chem. Phys.* **1981**, *74*, 2774.
(46) Edwards, S. F. *Proc. Phys. Soc., London* **1966**, *88*, 265.
(47) Jannink, G.; de Gennes, P. G. *J. Chem. Phys.* **1968**, *48*, 2260.
(48) The type of interpenetration that occurs in semidilute solutions of monodisperse linear polymers is not appropriate here; indeed it would yield a mesh size ξ that would remain independent of the polymer sizes and could not show the observed growth with reaction time.
(49) Dietler, G.; Aubert, C.; Cannell, D. S.; Wiltzius, P. *Phys. Rev. Lett.* **1986**, *24*, 3117.
(50) Vacher, R.; Woignier, T.; Pelous, J.; Courtens, E. *Phys. Rev. B: Condens. Matter* **1988**, *37*, 6500.
(51) Martin, J. E. In *Time Dependent Effects in Disordered Systems*; Pynn, R., Riste, T., Eds.; NATO ASI Series B: Physics; Plenum, New York, 1987; Vol 167.
(52) Hermann, H. J.; Kolb, M. *J. Phys. A: Math. Gen.* **1986**, *19*, L1027.

Notes

^{13}C Solid-State NMR of Solution-Prepared Polymorphs of Poly(α-isobutyl L-aspartate)

R. A. QUINTERO-ARCAYA, F. A. BOVEY,* J. M. FERNANDEZ-SANTIN,† and J. A. SUBIRANA

AT&T Bell Laboratories, Murray Hill, New Jersey 07974.
Received September 26, 1988;
Revised Manuscript Received January 19, 1989

Two solid forms of poly(α-isobutyl L-aspartate) (PAIBLA, **1**), have recently been prepared.[1] The X-ray diffraction patterns and morphological characteristics (orientability) of these solid phases point to two distinctly different solid-state structures. While PAIBLA may be regarded as a derivative of nylon 3, it may also be thought of as a polypeptide into the main chain of which a methylene unit has been added. The X-ray diffraction diagrams of the two forms of PAIBLA can be interpreted in terms of helical structures held together by systems of hydrogen bonds similar to those found in α-helical polypeptides. Model studies[1a] have allowed the selection of some possibilities for the conformational state of the monomer unit in either of the two solid forms.

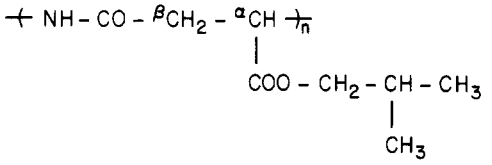

1

Studies of polypeptides have been reported using ^{13}C NMR in the solid state,[2] and it has been found that, as in solution,[3] the ^{13}C chemical shifts are sensitive to chain conformation. We have performed such experiments on PAIBLA, employing magic-angle spinning with ^1H–^{13}C cross-polarization and dipolar decoupling (abbreviated MAS-CP-DD).[4] It was our hope that such measurements might be informative concerning both chain conformation and dynamics in the two seemingly different crystalline forms. PAIBLA is also distinguished from polypeptides in having a substantial amorphous fraction, and it appeared that ^{13}C NMR might be useful in characterizing this phase.

†CSIC, Escuela Técnica Superior de Ingenieros Industriales de Barcelona, Diagonal 647, Barcelona 08028, Spain.

Experimental Section

Sample. The polymer used in this study was obtained by a slight modification of the preparative procedure reported previously:[1a] isobutyl alcohol was added instead of sodium isobutoxide. The degree of polymerization is approximately 800. Depending on the manner in which a chloroform solution of the polymer is treated, two solid forms may be obtained:[1a]

Form A. When ethanol is added to a chloroform solution of the polymer,[1a] a powder precipitates. Even though single crystals of this form have been grown, no fibers have yet been obtained from this material.

Form B. A film of this form is prepared by drying a chloroform solution of the polymer. The orientability of form B distinguishes this solid phase from form A.

Calorimetric Measurements. An amount of 3.22 mg of form A was heated, at a rate of 10 deg/min, on a Perkin-Elmer DSC-4.

NMR Measurements. All measurements were carried out at 50.31 MHz on a Varian XL-200 instrument. The probe and Al_2O_3 rotor were manufactured by Doty Scientific, Inc. Pulses at 90° of 5.3-μs duration were employed with an interval between pulses of 3 s. The scalar proton decoupling (SD) was carried out at a B_2 field strength ($\gamma B_2/2\pi$) of 4400 Hz or ca. 1 G. The high-power proton decoupling (DD) field was 45 kHz or ca. 11 G. All spectra were observed at 24 °C; spin–lattice relaxation times were measured at 21° by using the cross polarization method of Torchia.[5]

Results and Discussion

The MAS-CP-DD carbon-13 spectra of the two forms are shown in Figure 1. The assignment of resonances was made by comparison to solution spectra.[6] At this field, amide and ester carbonyl resonances are not resolved in the solid state. (At ca. 100° a partial resolution is observed, resulting in a high-field shoulder on the carbonyl resonance; this may be the ester carbonyl.) The carbon-13 spectrum of form A shows a markedly greater signal-to-noise ratio than that of form B. This is evident from a comparison of spectra a and b in Figure 1. Since the same amount of sample (50 mg) was used for both experiments, this observation suggests a higher degree of crystallinity for form A, but a quantitative measurement was not carried out.

The most significant observation is that the main-chain carbon chemical shifts are identical for both forms (Table I) within experimental error (±0.5 ppm). The sensitivity of carbon-13 chemical shifts to changes in conformation has been thoroughly established both in solution and in the solid state (see, for example, ref 2 and 3). Polypeptides in the solid state show different chemical shifts for the β-sheet and α-helical forms.[2,7–9] Particularly relevant to

0024-9297/89/2222-2533$01.50/0